

Spin Squeezing Enhanced Quantum Magnetometry with Nitrogen-Vacancy Center Qutrits

Lea Gassab^{1,*} and Özgür E. Müstecaplıoğlu^{1,2,3}

¹*Department of Physics, Koç University, 34450 Sarıyer, İstanbul, Türkiye*

²*TÜBİTAK Research Institute for Fundamental Sciences, 41470 Gebze, Türkiye*

³*Faculty of Engineering and Natural Sciences, Sabancı University, 34956 Tuzla, İstanbul, Türkiye*

We explore the utility of quantum spin squeezing in quantum magnetometry, focusing on three-level (qutrit) Nitrogen-Vacancy (NV) centers within diamond, utilizing a standard Ramsey interferometry pulse protocol. Our investigation incorporates the effects of dephasing and relaxation on NV centers' dynamics during Ramsey measurements, modeled via the Lindblad quantum master equation. We conduct a comparative analysis between the metrological capabilities of a single NV center and a pair of NV centers, considering Quantum Fisher Information both with and without spin squeezing. The quantum correlations between NV centers are assessed through the evaluation of the Kitagawa-Ueda spin squeezing parameter within a two-level manifold. Additionally, parallel calculations are conducted using a two-level model (qubit) for NV centers. Our findings reveal that leveraging qutrits and spin squeezing yields enhanced magnetometric precision, albeit constrained by dephasing effects. Nevertheless, even in the absence of dynamical decoupling methods to mitigate environmental noise, strategic timing of squeezing and free evolution can sustain the advantages of qutrit-based magnetometry.

I. INTRODUCTION

The exploration of precisely controlled quantum systems as highly sensitive nanoscale detectors holds significant promise in advancing our comprehension of intricate processes within biological and condensed-matter systems, operating at molecular and atomic scales [1, 2]. The demanding criteria for both high sensitivity and spatial resolution have prompted suggestions to employ spin-based quantum systems as nanoscale magnetometers [3] or to utilize imaging through the detection of sample-induced decoherence [4]. A particularly appealing physical platform for realizing these concepts is the Nitrogen-Vacancy (NV) center in diamond. This choice is motivated by the center's prolonged coherence times at room temperature and its convenient optical readout of the spin state [5–10].

Given the considerable potential of the NV center, researchers have conducted studies to enhance the sensing capabilities of this probe. Specific pulse sequences, such as Carr-Purcell-Meiboom-Gill (CPMG) and Dynamic Decoupling (DD) [11, 12], have been used to prolong coherent time. Additionally, researchers have investigated the use of entangled NV centers [13, 14] and, finally, spin squeezing [15]. Spin squeezing, as introduced by Kitagawa and Ueda [16], involves the quantum redistribution of uncertainties along two orthogonal spin directions. This operation holds significance in quantum sensing and metrology, providing a means to enhance measurement precision beyond the standard quantum limit in experiments [17–19]. Consequently, spin squeezing emerges as a valuable resource in applications of quantum technology. In the context of spin squeezing generation for NV centers, ensembles of qubits are typically considered. However, this approach has limitations as the qubit model is an approximation that necessitates a bias field. Here, we explore the potential of using qutrits for NV centers. Pulsed dynamical generation of spin squeezing has been explored in the literature for spin-1 systems [20, 21] and other methods, including generation

via nonadiabatic control [22]. In the context of NV centers, Ramsey interferometry is recognized as a straightforward and efficient protocol for measuring magnetic fields. It has been extensively studied in qubit systems [23–26] and has also been discussed for qutrit systems [27, 28].

In this article, we explore the potential enhancements in quantum metrological performance achievable by transitioning from two-level (qubits) to three-level (qutrits) spin systems and incorporating spin squeezing within typical quantum magnetometry settings, specifically NV center Ramsey interferometry. We adopt a foundational approach, comparing qubit versus qutrit Ramsey quantum magnetometry scenarios, both with and without spin squeezing, in terms of Quantum Fisher Information (QFI). Considering the influence of quantum dephasing and relaxation during the spin system's evolution, our findings suggest that qutrits, coupled with the additional step of spin squeezing, can outperform qubits in terms of QFI, provided that the spin squeezing magnitude, the timing of squeezing and free evolution are optimally determined.

The structure of the paper is as follows: Section II provides an overview of the employed model, elucidating the Hamiltonian and dynamics. In Section III, we introduce QFI and spin squeezing parameter. Section IV presents our results, and finally, Section V summarizes our conclusions.

II. MODEL

In a scenario where there exists an unknown, potentially weak magnetic field within a defined region, our objective is to measure this magnetic field with the utmost precision possible. To accomplish this, we utilize one or two NV centers as our probes. The NV center, characterized as an optically active color defect, results from a substitutional nitrogen impurity and a neighboring carbon vacancy in the diamond lattice. Comprising six electrons from nitrogen and the surrounding carbon atoms, the negatively charged NV center is described as a spin-1 system. We opt to explore the full capabilities of the NV center by modeling it as a qutrit system. This choice is motivated by the potential advantages that qutrits offer in

* lgassab20@ku.edu.tr

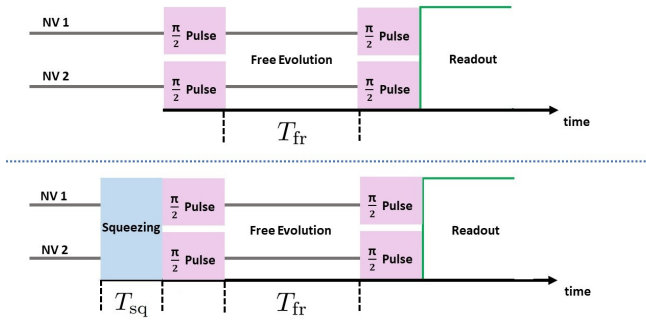


Figure 1. The application of Ramsey-type sequence on two Nitrogen-Vacancy (NV) Centers with and without the introduction of spin squeezing. T_{fr} is the free evolution time. T_{sq} is the duration of the application of spin squeezing.

metrology when compared to qubits [29, 30]. Its ground state is a spin triplet (3A_2) denoted as $|Sm_S\rangle$ with $S = 1$ and $m_S = 0, \pm 1$. The NV center Hamiltonian captures these properties, while the excited-state triplet (3E) is acknowledged at a higher energy level and is not explored in this context [31, 32].

Initially, our focus is on a single NV center. We then extend our consideration to two NV centers, exploring Ramsey interferometry with and without the application of spin squeezing as illustrated in Fig. 1.

A. Free Hamiltonian and Initial states

Neglecting interactions with nuclear spins or spin-strain effects [33, 34], the Hamiltonian governing N NV centers is expressed as follows,

$$\hat{H}_0 = \sum_{i=1}^N \left[D \hat{S}_{zi}^2 + g_S \vec{B} \cdot \vec{\hat{S}}_i \right]. \quad (1)$$

We take $\hbar = 1$ here and in the rest of the paper. $D = 2.87$ GHz is the temperature-dependent zero-field splitting, and $g_S = 1.80$ MHz/G is the gyromagnetic ratio for the electron spin. The magnetic field taken parallel to the NV center axis (z) is denoted as $\vec{B} = (0, 0, B_z)$. The spin-1 operator $\vec{\hat{S}} = (\hat{S}_x, \hat{S}_y, \hat{S}_z)$ is defined as

$$\hat{S}_x = \frac{\hbar}{\sqrt{2}} \begin{bmatrix} 0 & 1 & 0 \\ 1 & 0 & 1 \\ 0 & 1 & 0 \end{bmatrix}, \quad (2)$$

$$\hat{S}_y = \frac{\hbar}{\sqrt{2}} \begin{bmatrix} 0 & -i & 0 \\ i & 0 & -i \\ 0 & i & 0 \end{bmatrix}, \quad (3)$$

$$\hat{S}_z = \hbar \begin{bmatrix} 1 & 0 & 0 \\ 0 & 0 & 0 \\ 0 & 0 & -1 \end{bmatrix}. \quad (4)$$

\hat{S}_i is the spin matrix for the i^{th} NV center. Due to the Zeeman effect in the presence of a magnetic field, the electron spin

($S = 1$) is split into three states: $m_s = 0, 1, -1$, denoted as $|0\rangle, |1\rangle$ and $| -1 \rangle$. The initial state of the NV center is taken in the excited state $| -1 \rangle$,

$$|\psi_0\rangle = \bigotimes_{i=1}^N | -1 \rangle. \quad (5)$$

Then, each NV center undergoes a $\pi/2$ pulse, achieved by applying a rotation operator,

$$e^{-i\frac{\pi}{2}\hat{S}_x}.$$

This pulse is experimentally generated by microwave drives [35].

When incorporating spin squeezing, the initial state, $|\psi_0\rangle$, is first driven through spin squeezing, and then subjected to the $\pi/2$ pulse, as illustrated in Fig. 1.

B. Spin Squeezing Generation

To describe the intricate dynamics and capture the squeezing effects in the Hamiltonian for two NV centers, a squeezing term is introduced [36],

$$\hat{H}_S = c_1 \left(\sum_{i=1}^N \hat{S}_{xi} \right)^2, \quad (6)$$

where c_1 is the squeezing constant. The Hamiltonian, as depicted in Eq. (6), is referred as a one-axis twisting Hamiltonian. The choice of x -axis twisting in the context of spin squeezing is strategic, as it allows for the manipulation of the noise cone, effectively narrowing the error ellipse of the spin. This, combined with the optimal initial state, enhances the precision of the magnetic field measurement by interplaying with the z -axis rotation induced by the magnetic field [37].

The generation of this type of Hamiltonian in real setup has been discussed in the literature. It can be realized through phonon mediation, as evidenced in [38] or produced in optical cavities [39]. In our specific protocol, we need to deactivate spin squeezing after a specific duration. A dynamic control method for NV center spin squeezing, as discussed in [40], could potentially address the technical challenge.

Alternative approaches to generating spin squeezing have been proposed. One example involves using microwave fields in silicon-vacancy centers, which are similar to NV centers [41]. Additionally, a universal method, introduced in [21], is also applicable to NV centers. The method presents a generic scheme for creating spin squeezing in any non-squeezing systems through the use of periodic rotation pulses.

C. Dynamics

We describe the open quantum system dynamics of the NV center by the following Lindblad master equation [42],

$$\dot{\rho}(t) = -i[\hat{H}, \rho(t)] + \mathcal{D}_t(\rho(t)) + \mathcal{D}_d(\rho(t)), \quad (7)$$

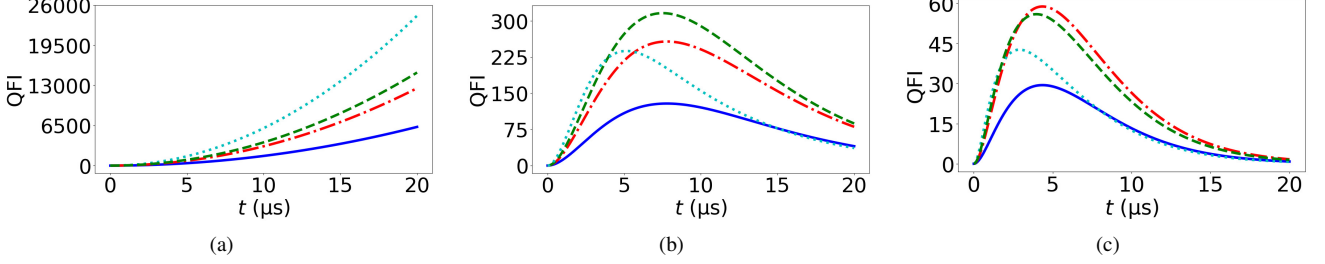


Figure 2. The Quantum Fisher Information (QFI) as a function of time with $B = 50$ G for the spin-1 formalism. The curves represents the free evolution as follows: the solid blue curve corresponds to a single NV center, the dashed-dotted red curve corresponds to two NV centers, the pointed cyan curve represents two NV centers subjected to spin squeezing ($c_1 = 2.5$ GHz, $T_{\text{sq}} = 3$ ns), and the dashed green curve represents two NV centers subjected to spin squeezing ($c_1 = 0.25$ GHz, $T_{\text{sq}} = 30$ ns). The different scenarios are illustrated as: (a) without including any noise terms, (b) including thermalization and dephasing with $\gamma_t = 0.2$ MHz and $\gamma_d = 0.1\gamma_t$, and (c) including thermalization and dephasing with $\gamma_t = 0.2$ MHz and $\gamma_d = \gamma_t$.

where the unitary contribution to the dynamics, \hat{H} , is provided as follows,

- during free evolution by $\hat{H} = \hat{H}_0$,
- during spin squeezing by $\hat{H} = \hat{H}_0 + \hat{H}_S$.

The NV center, while a robust quantum system, is inevitably influenced by the fluctuating states of nearby nuclear spins. These nuclear spins introduce a dynamic and unpredictable backdrop, contributing to the environmental noise that impacts the precision of measurements performed on the NV center. We assume very low temperatures relative to the NV center transition frequencies. Dephasing and thermalization are incorporated through the dissipators given as follows,

$$\mathcal{D}_d(\rho) = \sum_{i=1}^N \gamma_d [\hat{S}_{zi} \rho(t) \hat{S}_{zi} - \rho(t)]; \quad (8)$$

$$\mathcal{D}_t(\rho) = \sum_{i=1}^N \gamma_t \left[\hat{S}_i^- \rho(t) \hat{S}_i^+ - \frac{1}{2} \left\{ \hat{S}_i^+ \hat{S}_i^-, \rho(t) \right\} \right], \quad (9)$$

where \hat{S}_i^- is the lowering operator of the i^{th} NV center, and,

$$\hat{S}^- = \frac{1}{2} (\hat{S}_x - i\hat{S}_y). \quad (10)$$

We define the thermalization rate, denoted by γ_t , as $20 \mu\text{s}$, based on the literature [43]. For the dephasing rate, γ_d , we will consider two scenarios: one where γ_d is 10% of the thermalization rate ($\gamma_d = 0.1\gamma_t$), and another where it is equal to the thermalization rate ($\gamma_d = \gamma_t$).

III. QUANTUM MEASURES

A. Quantum Fisher Information

In the context of quantum parameter estimation, particularly for magnetic field sensing, fundamental results in quantum metrology become imperative. Let us consider a scenario

where a quantum state encodes a parameter θ , and the goal is to estimate this parameter with optimal precision [44, 45]. For a mixed state described by the density operator, $\hat{\rho}$, the QFI can be defined, using the Symmetric Logarithmic Derivative (SLD) operator (\hat{L}_θ), as

$$F_Q(\theta) = \text{Tr}[\hat{\rho} \hat{L}_\theta^2]. \quad (11)$$

The SLD operator is implicitly determined by the equation,

$$\partial_\theta \hat{\rho} = \frac{\hat{L}_\theta \hat{\rho} + \hat{\rho} \hat{L}_\theta}{2}. \quad (12)$$

Expressing \hat{L}_θ in the eigenbasis of $\hat{\rho}$, the QFI takes the form,

$$F_Q(\theta) = 2 \sum_{k,l} \frac{|\langle k | \partial_\theta \hat{\rho} | l \rangle|^2}{\lambda_k + \lambda_l}. \quad (13)$$

Here, $|k\rangle$ and $|l\rangle$ are the eigenvectors and λ_k and λ_l are the eigenvalues of the density operator $\hat{\rho}$.

In the specific application of estimating a magnetic field, θ , in our case, is the strength of the magnetic field, and the QFI provides a quantitative measure of the ultimate precision achievable in such quantum magnetic field sensing experiments. This theoretical foundation is critical for understanding the limits and potential advancements in quantum-enhanced magnetic field measurements. To quantify this precision, we employ the QuanEstimation toolbox in Python [46] to calculate the QFI.

B. Spin Squeezing Parameter

The concept of spin squeezing is established by defining it as the condition where the variance of a spin component normal to the mean spin is smaller than the standard quantum limit. To quantify the extent of spin squeezing, we employ the spin squeezing parameter, as introduced by Kitagawa and Ueda [16]. Kitagawa-Ueda spin squeezing brings quantum entanglement perspective to the usual spin squeezing which is the reduction of spin noise in a certain direction at the cost of

more noise in other directions. This criterion is given by

$$\xi^2 = \frac{4(\Delta\hat{J}_{n_\perp}^2)_{\min}}{N}, \quad (14)$$

where n_\perp is an axis perpendicular to the mean-spin direction \hat{n} , N is the number of spins (in our case, $N = 2$), and \hat{J} represents the collective spin operator. Kitagawa-Ueda and other quantum correlations based criteria of spin squeezing [47] are commonly defined for SU(2) or spin-1/2 atomic ensembles. Spin squeezing in SU(3) or spin-1 systems can be discussed in their SU(2) subgroups, such as isospin squeezing [48]. We follow a similar approach to characterize quantum correlations and spin squeezing within the manifold of $\{|0\rangle, | -1\rangle\}$. In general, spin squeezing can be optimized by rotating the coordinate frame and choosing the critical rotation angles. For simplicity, we only consider a fixed reference frame. Based on this manifold, the spin matrices $\hat{\sigma} = (\hat{\sigma}_x, \hat{\sigma}_y, \hat{\sigma}_z)$ are written as

$$\hat{\sigma}_x = |0\rangle\langle -1| + | -1\rangle\langle 0|, \quad (15)$$

$$\hat{\sigma}_y = i(|0\rangle\langle -1| - | - 1\rangle\langle 0|), \quad (16)$$

$$\hat{\sigma}_z = | - 1\rangle\langle - 1| - |0\rangle\langle 0|, \quad (17)$$

and the collective spin $\hat{J} = (\hat{J}_x, \hat{J}_y, \hat{J}_z)$ is defined as

$$\hat{J}_x = \frac{1}{2}(\hat{\sigma}_x \otimes I_3 + I_3 \otimes \hat{\sigma}_x), \quad (18)$$

$$\hat{J}_y = \frac{1}{2}(\hat{\sigma}_y \otimes I_3 + I_3 \otimes \hat{\sigma}_y), \quad (19)$$

$$\hat{J}_z = \frac{1}{2}(\hat{\sigma}_z \otimes I_3 + I_3 \otimes \hat{\sigma}_z), \quad (20)$$

with I_3 being the three-dimensional unit matrix. To calculate spin squeezing, we calculate the mean spin squeezing direction \hat{n} for the state,

$$\hat{n} = \frac{(\langle \hat{J}_x \rangle, \langle \hat{J}_y \rangle, \langle \hat{J}_z \rangle)}{|\langle \hat{J} \rangle|}. \quad (21)$$

And then, we take the minimal variance, $(\Delta\hat{J}_{n_\perp}^2)_{\min}$, in the perpendicular direction of \hat{n} . The presence of spin squeezing is characterized by $\xi^2 < 1$. Spin squeezing is closely tied to the creation of entanglement [37, 49, 50]. Additionally, a previous study suggests that initial squeezing can aid in entanglement [51]. Our results are consistent with this statement (Appendix A).

IV. RESULTS

In our simulations, the magnetic field was fixed at $B = 50$ G, but similar results were obtained across a range of values from 5 to 500 G. Initially, we investigate the typical Ramsey sequence for one and two NV centers, both starting in the initial state (Eq. 5). Subsequently, after a $\pi/2$ pulse, we allow the system to undergo evolution through the free Hamiltonian \hat{H}_0 for a duration of $T_{\text{fr}} = 20 \mu\text{s}$, T_{fr} being the free evolution time.

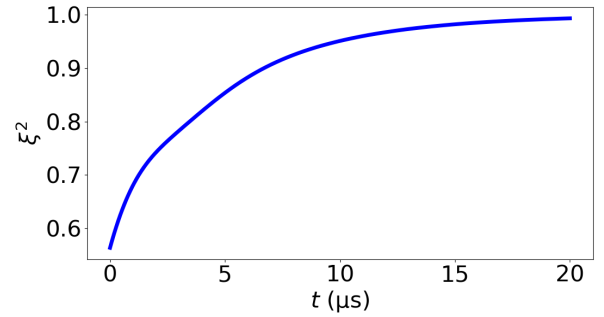


Figure 3. For the spin-1 formalism, the curve in solid blue represents the squeezing parameter, ξ^2 , as a function of time during the free evolution of two NV centers subjected to spin squeezing with $c_1 = 2.5$ GHz for a time of $T_{\text{sq}} = 3$ ns, including thermalization and dephasing with $\gamma_t = 0.2$ MHz, $\gamma_d = 0.1\gamma_t$, and $B = 50$ G.

We choose this time taking into account the dissipative time that falls within the order of tenth of microseconds. To further enhance precision, we start again in the initial state (Eq. 5), however before the $\pi/2$ pulse and the free evolution, we introduce spin squeezing for a duration of T_{sq} which corresponds to the time it takes for the squeezing parameter to reach its minimum value. The two scenarios are illustrated in Fig. 1.

A. Analysis with spin-1 formalism

Fig. 2 compares one NV center without spin squeezing (blue), two NV centers without spin squeezing (red) and two NV centers with spin squeezing applied at varying strengths, specifically with squeezing constants of $c_1 = 0.25$ GHz (green) and $c_1 = 2.5$ GHz (cyan).

In the case without spin squeezing, Fig. 2a shows a twofold increase in the QFI when transitioning from one NV center to two NV centers. When environmental noise is introduced (Fig. 2b and Fig. 2c), whether the QFI increases or decreases for one NV center, the twofold enhancement persists for two NV centers.

In the case with spin squeezing, in the absence of noise (Fig. 2a), the QFI is larger when spin squeezing is applied with squeezing constant, $c_1 = 0.25$ GHz. It increases further with a higher squeezing constant, $c_1 = 2.5$ GHz. When environmental noise is introduced with $\gamma_d = 0.1\gamma_t$ (Fig. 2b), spin squeezing remains beneficial, particularly at a lower squeezing constant, $c_1 = 0.25$ GHz. This suggests that in the presence of noise, a higher squeezing constant does not necessarily lead to higher QFI. Instead, a low squeezing constant ($c_1 = 0.25$ GHz), which is sufficient enough to generate spin squeezing, is more advantageous. However, within the first $4 \mu\text{s}$, a higher squeezing constant, $c_1 = 2.5$ GHz, provides more benefit.

Finally, Fig. 2c shows that the advantage of squeezing is lost when the dephasing rate increases to $\gamma_d = \gamma_t$. While spin squeezing enhance magnetic sensing capabilities, they are also highly sensitive to environmental noise, particularly dephasing. Analyzing the behavior of the QFI curves under such noise conditions is crucial. By identifying the time at which

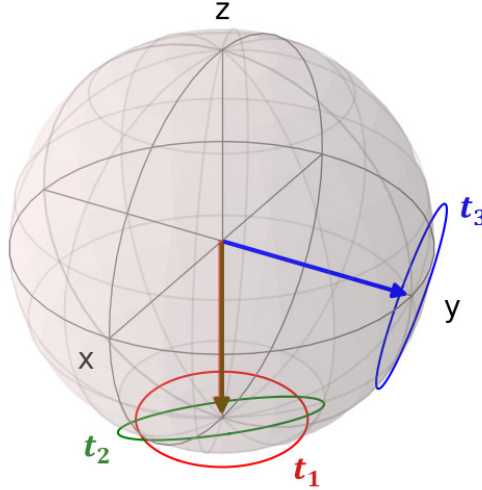


Figure 4. Illustration of the mean spin orientation and the variance of state preparation before the free evolution of the NV centers. At time t_1 , the state is in its initial configuration (Eq. (5)) with homogeneous variance. At time t_2 , the state reaches the end of the spin squeezing period, remaining aligned in the z -direction but with noise squeezed into an ellipse. Finally, at t_3 , a $\pi/2$ pulse is applied, shifting the state into the x - y plane.

the QFI reaches its maximum, we can optimize experimental design and ensure measurements are performed at the peak sensitivity. Experimentally, we typically measure populations or (\hat{S}_z) values. However, it is important to note that while the QFI is calculated for the optimal Positive Operator-Valued Measure (POVM), specifically the eigenprojectors of the SLD, measuring \hat{S}_z could potentially be suboptimal.

The effect of spin squeezing on the NV centers is further illustrated in Fig. 3. The squeezing parameter, initially around 0.5 (below 1) at the beginning of free evolution, increases due to dephasing and thermalization during this period. Appendix A demonstrates that spin squeezing also leads to entanglement.

Furthermore, given the initial state is oriented along the z -axis, when spin squeezing is applied, it reduces the variance in a specific direction, creating an ellipsoid shape that remains aligned with the z -axis. A $\pi/2$ pulse then shifts the spin into the x - y plane while preserving this variance ellipsoid. The effect of the magnetic field B is to precess the spin around the z -axis, and the x -axis twisting deforms the noise cone, effectively narrowing the spin's error ellipse. This sequence is illustrated in Fig. 4.

B. Analysis with spin-1/2 formalism

In this section, we examine the outcomes within the identical parameter scope for the spin-1/2 framework. This is achieved by concentrating on the dynamics of the states $|0\rangle$ and $|-\rangle$.

The Hamiltonian, in this context, is characterized as follows,

$$\hat{H}_0 = \sum_{i=1}^N \frac{\omega}{2} \hat{\sigma}_{zi}, \quad (22)$$

where $\omega = D - g_S B_z$ and $\hat{\sigma}_i = (\hat{\sigma}_{xi}, \hat{\sigma}_{yi}, \hat{\sigma}_{zi})$ are the Pauli matrices for the i^{th} NV center. The parameters and open quantum system dynamics are kept same as in the spin-1 model. Eq. (8) and Eq. (9) are modified respectively to

$$\mathcal{D}_d(\rho) = \sum_{i=1}^N \gamma_d [\hat{\sigma}_{zi} \rho(t) \hat{\sigma}_{zi} - \rho(t)]; \quad (23)$$

$$\mathcal{D}_t(\rho) = \sum_{i=1}^N \gamma_t [\hat{\sigma}_i^- \rho(t) \hat{\sigma}_i^+ - \frac{1}{2} \{\hat{\sigma}_i^+ \hat{\sigma}_i^-, \rho(t)\}], \quad (24)$$

where $\hat{\sigma}_i^\pm$ are the Pauli spin ladder operators for the i^{th} NV center. The spin squeezing Hamiltonian in Eq. (6) is modified to

$$\hat{H}_S = c_1 \left(\sum_{i=1}^N \hat{\sigma}_{xi} \right)^2. \quad (25)$$

The initial state of the NV center is taken in the excited state $|-\rangle$. Then each NV center undergoes an $\pi/2$ pulse, achieved by applying a rotation operator,

$$e^{-i\frac{\pi}{2}\hat{\sigma}_x}.$$

As in the spin-1 formalism, if spin squeezing is added, it is applied before the $\pi/2$ pulse. We then proceed to analyze the QFI under both scenarios (with and without squeezing), considering the presence and absence of noise.

In Fig. 5a, we observe that without considering any noise channel, spin squeezing yields a higher QFI. However, in the presence of noise (Fig. 5b and Fig. 5c), the advantages of spin squeezing are lost even for small dephasing (Fig. 5b), and Ramsey sequence without spin squeezing is more beneficial. Earlier in Fig. 2b, for the qutrit case, we observed advantages even in the presence of dephasing. Therefore, the benefits of using qutrit sensors over qubit sensors are clearly evident.

V. CONCLUSION

We have examined the potential of Nitrogen-Vacancy (NV) centers as quantum sensors for magnetic fields, exploring various scenarios involving single and paired NV centers using both qubit and qutrit models, and employing spin squeezing within Ramsey or Ramsey-type pulse sequence protocols. Throughout our investigation, we have analyzed the dynamics of Quantum Fisher Information (QFI) across these scenarios, utilizing the Lindblad master equation to model the spin system's evolution under dephasing and thermalizing noise.

Incorporating a spin squeezing step in magnetometric measurement and utilizing qutrit NV centers have demonstrated a precision increase relative to standard Ramsey magnetometry.

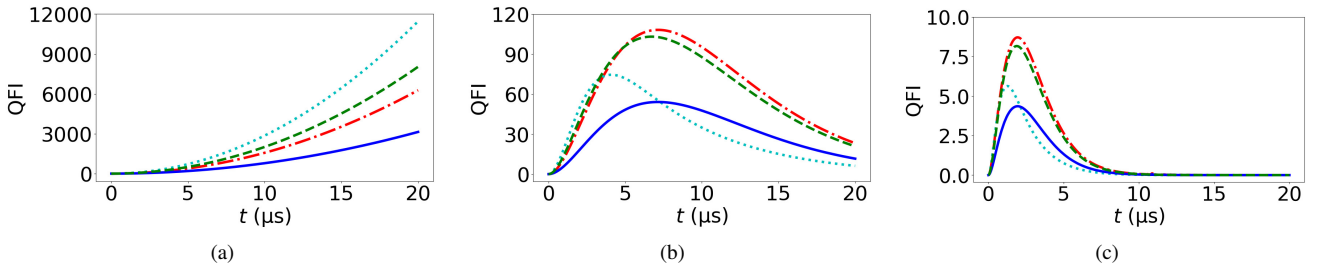


Figure 5. The Quantum Fisher Information (QFI) as a function of time with $B = 50$ G for the spin-1/2 formalism. The curves represents the free evolution as follows: the solid blue curve corresponds to a single NV center, the dashed-dotted red curve corresponds to two NV centers, the pointed cyan curve represents two NV centers subjected to spin squeezing ($c_1 = 2.5$ GHz, $T_{\text{sq}} = 3$ ns), and the dashed green curve represents two NV centers subjected to spin squeezing ($c_1 = 0.25$ GHz, $T_{\text{sq}} = 30$ ns). The different scenarios are illustrated as: (a) without including any noise terms, (b) including thermalization and dephasing with $\gamma_t = 0.2$ MHz and $\gamma_d = 0.1\gamma_t$, and (c) including thermalization and dephasing with $\gamma_t = 0.2$ MHz and $\gamma_d = \gamma_t$.

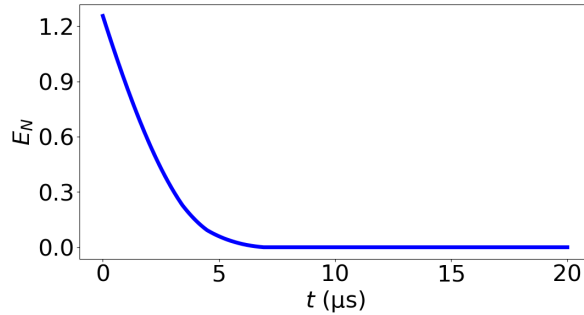


Figure 6. For the spin-1 formalism, the curve in solid blue represents the logarithmic negativity, E_N , as a function of time during the free evolution of two NV centers subjected to spin squeezing with $c_1 = 2.5$ GHz for a time of $T_{\text{sq}} = 3$ ns, including thermalization and dephasing with $\gamma_t = 0.2$ MHz, $\gamma_d = 0.1\gamma_t$, and $B = 50$ G.

However, the advantage of spin squeezing is notably sensitive to the dephasing environment. Our numerical analysis showed that, as dephasing increases, the advantages become marginal compared to standard methods. We also observed that moderate squeezing results in higher QFI compared to strong squeezing, which is only beneficial for a brief period of free evolution. Furthermore, by conducting the entire analysis using the spin-1/2 formalism and comparing it with the spin-1 formalism, we have demonstrated the advantages of utilizing a qutrit system over a qubit system.

Additionally, we have observed that spin squeezing is accompanied by the generation of entanglement, aligning with the general expectation of quantum entanglement as a metrological resource. However, further investigation is needed to determine whether it is spin noise distribution or entanglement alone that causes the precision limit enhancement. Our findings contribute to the broader exploration of quantum technologies beyond qubits, where qutrits and higher-dimensional qubits (qudits) are increasingly considered, particularly in the context of quantum computing [52, 53]. An intriguing question persists regarding the scalability, as

outlook in [54], of these advantages, especially regarding the utilization of NV center qutrit ensembles or the investigation of higher-level systems (qudits). These avenues pose exciting challenges for future studies, promising further insights.

ACKNOWLEDGEMENTS

This work was supported by the Scientific and Technological Research Council of Türkiye (TÜBİTAK) under Project Number 123F150. L. G. and Ö. E. M. thank TÜBİTAK for their support.

Appendix A: Entanglement Measure

For higher-dimensional systems than qubits, some entanglement measures exist. The negativity, denoted as $N(\rho_{AB})$, quantifies entanglement in bipartite quantum systems ρ_{AB} [55]. It is defined as the absolute sum of the negative eigenvalues of the partially transposed density matrix ρ_A^T ,

$$N(\rho_{AB}) = \sum_i |\lambda_i|, \quad (\text{A1})$$

where λ_i are the negative eigenvalues of the density matrix ρ_A^T . The logarithmic negativity, denoted as $E_N(\rho_{AB})$, is related to the negativity and serves as a good indicator of the degree of entanglement in our system. It is defined as

$$E_N(\rho_{AB}) = \log_2(2N(\rho_{AB}) + 1). \quad (\text{A2})$$

In Fig. 6, we observe that the application of spin squeezing to the two NV centers system creates an entanglement between them. This entanglement is illustrated by an increase in the logarithmic negativity during the application of spin squeezing. During free evolution, this entanglement decreases due to environmental noise. Thus, the creation of spin squeezing in our spin-1 systems is accompanied by the creation of entanglement.

[1] K. Hasselbach, C. Veauvy, and D. Mailly, Microsquid magnetometry and magnetic imaging, *Physica C: Superconductivity* **332**, 140 (2000).

[2] J. Kirtley, M. Ketchen, K. Stawiasz, J. Sun, W. Gallagher, S. Blanton, and S. Wind, High-resolution scanning squid microscope, *Applied Physics Letters* **66**, 1138 (1995).

[3] B. M. Chernobrod and G. P. Berman, Spin microscope based on optically detected magnetic resonance, *Journal of applied physics* **97** (2005).

[4] J. H. Cole and L. C. Hollenberg, Scanning quantum decoherence microscopy, *Nanotechnology* **20**, 495401 (2009).

[5] C. L. Degen, F. Reinhard, and P. Cappellaro, Quantum sensing, *Reviews of modern physics* **89**, 035002 (2017).

[6] F. Jelezko and J. Wrachtrup, Single defect centres in diamond: A review, *physica status solidi (a)* **203**, 3207 (2006).

[7] G. Balasubramanian, P. Neumann, D. Twitchen, M. Markham, R. Kolesov, N. Mizuochi, J. Isoya, J. Achard, J. Beck, J. Tissler, *et al.*, Ultralong spin coherence time in isotopically engineered diamond, *Nature materials* **8**, 383 (2009).

[8] M. Hanks, M. Trupke, J. Schmiedmayer, W. J. Munro, and K. Nemoto, High-fidelity spin measurement on the nitrogen-vacancy center, *New Journal of Physics* **19**, 103002 (2017).

[9] S. Hong, M. S. Grinolds, L. M. Pham, D. Le Sage, L. Luan, R. L. Walsworth, and A. Yacoby, Nanoscale magnetometry with nv centers in diamond, *MRS bulletin* **38**, 155 (2013).

[10] R. Schiragh, K. Chang, M. Loretz, and C. L. Degen, Nitrogen-vacancy centers in diamond: nanoscale sensors for physics and biology, *Annual review of physical chemistry* **65**, 83 (2014).

[11] J. Shim, I. Niemeyer, J. Zhang, and D. Suter, Robust dynamical decoupling for arbitrary quantum states of a single nv center in diamond, *Europhysics Letters* **99**, 40004 (2012).

[12] Z.-H. Wang, G. De Lange, D. Ristè, R. Hanson, and V. Dobrovitski, Comparison of dynamical decoupling protocols for a nitrogen-vacancy center in diamond, *Physical Review B* **85**, 155204 (2012).

[13] Z. Qiu, U. Vool, A. Hamo, and A. Yacoby, Nuclear spin assisted magnetic field angle sensing, *npj Quantum Information* **7**, 39 (2021).

[14] T. Xie, Z. Zhao, X. Kong, W. Ma, M. Wang, X. Ye, P. Yu, Z. Yang, S. Xu, P. Wang, *et al.*, Beating the standard quantum limit under ambient conditions with solid-state spins, *Science Advances* **7**, eabg9204 (2021).

[15] S. Dooley, E. Yukawa, Y. Matsuzaki, G. C. Knee, W. J. Munro, and K. Nemoto, A hybrid-systems approach to spin squeezing using a highly dissipative ancillary system, *New Journal of Physics* **18**, 053011 (2016).

[16] M. Kitagawa and M. Ueda, Squeezed spin states, *Physical Review A* **47**, 5138 (1993).

[17] J. B. Brask, R. Chaves, and J. Kołodyński, Improved quantum magnetometry beyond the standard quantum limit, *Physical Review X* **5**, 031010 (2015).

[18] L. Buchmann, S. Schreppler, J. Kohler, N. Spethmann, and D. Stamper-Kurn, Complex squeezing and force measurement beyond the standard quantum limit, *Physical review letters* **117**, 030801 (2016).

[19] C. Gross, Spin squeezing, entanglement and quantum metrology with bose-einstein condensates, *Phys. B: At. Mol. Opt. Phys.* **45**, 103001 (2012).

[20] T. K. Begzjav and G. S. Agarwal, Squeezing of spin-1 quantum states via a one-axis twisting hamiltonian, *Physical Review A* **104**, 023706 (2021).

[21] L. Huang, F. Chen, X. Li, Y. Li, R. Lü, and Y. Liu, Dynamic synthesis of heisenberg-limited spin squeezing, *npj Quantum Information* **7**, 168 (2021).

[22] L. Xin, M. Chapman, and T. Kennedy, Fast generation of time-stationary spin-1 squeezed states by nonadiabatic control, *PRX Quantum* **3**, 010328 (2022).

[23] E. T. Güldeme and C. Bulutay, Wavelet-based ramsey magnetometry enhancement of a single nv center in diamond, arXiv preprint [10.48550/arXiv.2310.18959](https://arxiv.org/abs/10.48550/arXiv.2310.18959) (2023).

[24] N. Oshnik, P. Rembold, T. Calarco, S. Montangero, E. Neu, and M. M. Müller, Robust magnetometry with single nitrogen-vacancy centers via two-step optimization, *Physical Review A* **106**, 013107 (2022).

[25] R. Coto, H. T. Dinani, A. Norambuena, M. Chen, and J. R. Maze, Probabilistic magnetometry with a two-spin system in diamond, *Quantum Science and Technology* **6**, 035011 (2021).

[26] L. Rondin, J.-P. Tetienne, T. Hingant, J.-F. Roch, P. Maletinsky, and V. Jacques, Magnetometry with nitrogen-vacancy defects in diamond, *Reports on progress in physics* **77**, 056503 (2014).

[27] J. T. Oon, J. Tang, C. A. Hart, K. S. Olsson, M. J. Turner, J. M. Schloss, and R. L. Walsworth, Ramsey envelope modulation in nv diamond magnetometry, *Physical Review B* **106**, 054110 (2022).

[28] C. A. Hart, J. M. Schloss, M. J. Turner, P. J. Scheidegger, E. Bauch, and R. L. Walsworth, N-v-diamond magnetic microscopy using a double quantum 4-ramsey protocol, *Physical Review Applied* **15**, 044020 (2021).

[29] F. Yan, M. Yang, and Z.-L. Cao, Optimal reconstruction of the states in qutrit systems, *Physical Review A* **82**, 044102 (2010).

[30] A. Shlyakhov, V. Zemlyanov, M. Suslov, A. V. Lebedev, G. S. Paraoanu, G. B. Lesovik, and G. Blatter, Quantum metrology with a transmon qutrit, *Physical Review A* **97**, 022115 (2018).

[31] J. F. Barry, J. M. Schloss, E. Bauch, M. J. Turner, C. A. Hart, L. M. Pham, and R. L. Walsworth, Sensitivity optimization for nv-diamond magnetometry, *Reviews of Modern Physics* **92**, 015004 (2020).

[32] M. W. Doherty, N. B. Manson, P. Delaney, F. Jelezko, J. Wrachtrup, and L. C. Hollenberg, The nitrogen-vacancy colour centre in diamond, *Physics Reports* **528**, 1 (2013).

[33] V. K. Sewani, H. H. Vallabhapurapu, Y. Yang, H. R. Firgau, C. Adambukulam, B. C. Johnson, J. J. Pla, and A. Laucht, Coherent control of nv- centers in diamond in a quantum teaching lab, *American Journal of Physics* **88**, 1156 (2020).

[34] K. Ullah, E. Köse, R. Yagan, M. C. Onbaşlı, and Ö. E. Müstecaplıoğlu, Steady state entanglement of distant nitrogen-vacancy centers in a coherent thermal magnon bath, *Physical Review Research* **4**, 023221 (2022).

[35] G. Mariani, S. Nomoto, S. Kashiwaya, and S. Nomura, System for the remote control and imaging of mw fields for spin manipulation in nv centers in diamond, *Scientific reports* **10**, 4813 (2020).

[36] X. Wang and B. C. Sanders, Spin squeezing and pairwise entanglement for symmetric multiqubit states, *Physical Review A* **68**, 012101 (2003).

[37] G. Tóth, C. Knapp, O. Gühne, and H. J. Briegel, Spin squeezing and entanglement, *Physical Review A* **79**, 042334 (2009).

[38] S. D. Bennett, N. Y. Yao, J. Otterbach, P. Zoller, P. Rabl, and M. D. Lukin, Phonon-induced spin-spin interactions in diamond nanostructures: Application to spin squeezing, *Phys. Rev. Lett.* **110**, 156402 (2013).

[39] J. Borregaard, E. Davis, G. S. Bentsen, M. H. Schleier-Smith,

and A. S. Sørensen, One-and two-axis squeezing of atomic ensembles in optical cavities, *New Journal of Physics* **19**, 093021 (2017).

[40] W. Song, W. Yang, J. An, and M. Feng, Dissipation-assisted spin squeezing of nitrogen-vacancy centers coupled to a rectangular hollow metallic waveguide, *Optics Express* **25**, 19226 (2017).

[41] Y.-H. Ma, Y. Xu, Q.-Z. Ding, and Y.-S. Chen, Preparation of spin squeezed state in siv centers coupled by diamond waveguide, *Chinese Physics B* **30**, 100311 (2021).

[42] H.-P. Breuer, F. Petruccione, *et al.*, *The theory of open quantum systems* (Oxford University Press on Demand, 2002).

[43] C. Abeywardana, V. Stepanov, F. H. Cho, and S. Takahashi, Magnetic resonance spectroscopy using a single nitrogen-vacancy center in diamond, in *Quantum and Nonlinear Optics III*, Vol. 9269 (SPIE, 2014) pp. 27–33.

[44] S. Luo, Quantum fisher information and uncertainty relations, *Letters in Mathematical Physics* **53**, 243 (2000).

[45] J. Liu, H. Yuan, X.-M. Lu, and X. Wang, Quantum fisher information matrix and multiparameter estimation, *J. Phys. A: Math. Theor.* **F 53**, 023001 (2020).

[46] M. Zhang, H.-M. Yu, H. Yuan, X. Wang, R. Demkowicz-Dobrzański, and J. Liu, Quanestimation: An open-source toolkit for quantum parameter estimation, *Physical Review Research* **4**, 043057 (2022).

[47] J. Ma, X. Wang, C.-P. Sun, and F. Nori, Quantum spin squeezing, *Physics Reports* **509**, 89 (2011).

[48] Ö. E. Müstecaplıoğlu, M. Zhang, and L. You, Spin squeezing and entanglement in spinor condensates, *Physical Review A* **66**, 033611 (2002).

[49] S. Sirsi, Spin squeezing, entanglement and correlations, *J. Opt. B: Quantum Semiclass. Opt.* **6**, 437 (2004).

[50] G. Vitagliano, I. Apellaniz, I. L. Egusquiza, and G. Tóth, Spin squeezing and entanglement for an arbitrary spin, *Physical Review A* **89**, 032307 (2014).

[51] A. Pradana and L. Y. Chew, Entanglement of nitrogen-vacancy-center ensembles with initial squeezing, *Physical Review A* **104**, 022435 (2021).

[52] O. Ogunkoya, J. Kim, B. Peng, A. B. Özgüler, and Y. Alexeev, Qutrit circuits and algebraic relations: A pathway to efficient spin-1 hamiltonian simulation, *Physical Review A* **109**, 012426 (2024).

[53] Q. Xu, L.-X. Zhou, T.-F. Feng, S.-F. Qiu, S.-W. Li, W.-J. Zhang, H. Luo, and X.-Q. Zhou, Experimental quantum state compression from two identical qubits to a qutrit, *Sci. China Phys. Mech. Astron.* **67**, 270311 (2024).

[54] M. Adani, S. Cavazzoni, B. Teklu, P. Bordone, and M. G. Paris, Critical metrology of minimally accessible anisotropic spin chains, arXiv preprint arXiv:2405.20296 10.48550/arXiv.2405.20296 (2024).

[55] F. Benabdallah, H. A. Zad, M. Daoud, and N. Ananikian, Dynamics of quantum correlations in a qubit-qutrit spin system under random telegraph noise, *Physica Scripta* **96**, 125116 (2021).